Heterojunction of CuO nanoclusters with TiO 2 for photo-oxidation of organic compounds and for hydrogen production

Maria Guadalupe Méndez-Medrano, Ewa Kowalska, Bunsho Ohtani, Daniel Bahena Uribe, Christophe Colbeau-Justin, Sven Rau, José Luis Rodríguez-López, Hynd Remita

Heterojunction of CuO Nanoclusters with TiO_2 for Photo-Oxidation of Organic Compounds and for Hydrogen Production

Maria Guadalupe Méndez-Medrano,[a,b] Ewa Kowalska,[c] Bunsho Ohtani,[c] Daniel Bahena Uribe,[d] Christophe Colbeau-Justin,[a] Sven Rau,[e] Jose Luis Rodríguez-López,[b,] and Hynd Remita.[a,f,*]*

[a] *Institut de Chimie Physique, UMR 8000 CNRS, Université Paris-Saclay, 91405 Orsay, France.*
[b] *Advanced Materials Department, IPICYT, 78216 San Luis Potosi, SLP, Mexico.*
[c] *Institute for Catalysis, Hokkaido University, Sapporo 001-0021, Japan*
[d] *Centro de Investigación y de Estudios Avanzados del Instituto Politécnico Nacional, l07360, D.F., Mexico.*
[e] *Institute for Inorganic Chemistry 1, Ulm University, Albert-Einstein-Allee 11, 89081 Ulm, Germany.*
[f] *CNRS, Institut de Chimie Physique, UMR 8000, 91405 Orsay, France.*

**jlrdz@ipicyt.edu.mx; Tel : +52 444 834 2000 x 7217*
** hynd.remita@universite-paris-saclay.fr; Tel: +33 (0)1 69 15 72 58.*

Abstract

Heterojunctions of small CuO nanoclusters (synthesized by radiolysis) with TiO_2 (commercial P25) induced a photocatalytic activity under visible light irradiation in a wide range of wavelengths due to the narrow band gap of CuO nanoclusters of around 1.7 eV. The optical, chemical and electrical properties of these composite nanomaterials were studied. The photocatalytic properties of bare and modified TiO_2-P25 were studied for water purification (photooxidation of organic compounds such as phenol and 2-propanol) and for hydrogen generation under visible light irradiation. Time Resolved Microwave Conductivity (TRMC) signals showed the activation of TiO_2 under visible light, proving the injection of electrons from CuO nanoclusters to the conduction band (CB) of TiO_2-P25. The modified materials showed high photocatalytic activity under visible light. The important role of charge-carriers was demonstrated for both the photoreduction and photooxidation reactions.

1. Introduction

Titanium dioxide (TiO_2) is currently the most widely used photocatalyst because of its high photocatalytic activity, chemical and thermal stability, large scale production, low cost, and low-toxicity.[1,2,3] TiO_2 is an excellent photocatalyst for the decomposition of many organic compounds, and TiO_2 modified with metal nanoparticles (e.g., Cu, Au, Ag, Pt) can be efficient for hydrogen generation by alcohols' dehydrogenation.[4,5] However, TiO_2 has also some drawbacks: (1) high rate of charge-carrier recombinations, which leads to a low quantum efficiency, and (2) high value of the energy band gap for its crystalline phases (e.g., 3.2 eV and 3.1 eV for anatase and rutile, respectively),[6] which means that it can only be excited under UV or near-UV.[7] However, the solar spectrum is composed of only ca. 4% of UV light. Therefore, a lot of research is focused on the development of visible-light responsive photocatalysts for more efficient use of solar energy for energy conversion, hydrogen production by the water splitting process (PWS),[4,8] CO_2 reduction,[9] and water and air treatment.[10,11]

To enhance its photocatalytic activity under UV and visible light, TiO_2 has been doped with cations and ions of various elements (e.g., N, C, S…), surface modified with metal nanoparticles (such as, Au, Ag, Pt…) or associated to another semiconductors (SCs) (such as ZrO, ZnS, CdS, BiOCl, BiOBr, WO_3).[12] The heterojunctions with another semiconductor of a narrow band gap (NBG-SC) can lead to some advantages such as: i) photoactivity under visible irradiation, ii) better charge carrier separation,[13] iii) lower cost than metal modification, and iv) possible co-catalytic reactions.[14]

Less expensive materials like copper-based nanomaterials have attracted attention in the field of photocatalysis.[10,15,16,17] It has been proposed that coupling of TiO_2 (n- type semiconductor) with copper oxide (p-type semiconductor) of a narrow band gap (1.7 eV)[18] could overcome limitations of TiO_2 in terms of visible light absorption and charge-carrier recombinations, enhancing the photoactivity under UV irradiation, and principally under visible irradiation. However, it should be pointed out that titania modification with Cu-based bimetallic nanoparticles (NPs), e.g., Cu-Ag, Cu-Au, and Cu-Pt[10,15,16,17] does not always lead to an improvement in the photocatalytic activity. For example, it has been proposed that the deposition of two metals close to each other (e.g., core-shell nanostructures) can result in charge carriers' recombination (electron transfer between metallic deposits) instead of "hot" electron transfer from plasmonic metal nanoparticles (Ag-Cu and Ag-Au NPs) to the conduction band (CB) of titania.[19,20]

Copper has recently attracted a lot of attention because of its low cost, good conductivity and excellent antibacterial and antifungal properties. Recent studies have reported the promising

activity of Cu-based NPs as catalysts for hydrogen production and CO_2 reduction by photocatalysis.[4,21,22,23] Xu and Sun showed significant photoactivity of TiO_2 modified with CuO nanoparticles for H_2 generation from a water/methanol solution mixture.[14] In that study, the photocatalytic activity of CuO/TiO_2 was even higher than that of Pt/TiO_2 and CuO nanoparticles worked as an electron scavenger and co-catalysts for hydrogen prodution.[14] Other studies also reported that CuO/TiO_2 are also efficient photocatalysts for wastewater treatment, in the degradation of organic pollutants under visible light.[13,24,25]

Several chemical and physical routes have been used to prepare TiO_2-based composites. In aqueous solution, the methods of preparation involve impregnation method,[14] sol-gel, hydrothermal methods, and ionizing radiations (γ-rays, X-rays or electron or ion beams). Radiolysis is a very efficient technique to synthesize metal nanoparticles in solutions or on supports.[26,27,28,29] The radiolytic method presents the advantage of using simple physicochemical conditions such as, atmospheric pressure and room temperature, and of absence of contaminants. The method results in homogeneous reduction and nucleation leading to metal nanoparticles of controlled size.[30]

In this work, CuO nanoclusters (with different loading of Cu: 0.5-2 w%) have been synthesized on TiO_2 by radiolysis (gamma irradiation). The composite CuO-TiO_2 photocatalyst presents high photocatalytic activity under UV and more interestingly under visible light. Time Resolved Microwave Conductivity signals show that CuO nanoclusters, when excited by visible light, inject electrons in the conduction band of TiO_2 inducing a high photoactivity for organic pollutants' degradation and hydrogen production in a water/methanol mixture.

2. Experimental

2.1. Materials

As support material, titanium(IV) oxide (TiO_2), provided by Evonik (Commercial TiO_2-P25, with 50 m^2 g^{-1} of surface area and a crystalline composition of anatase (73-85%), rutile (14-17%) and amorphous titania (0-13%) [31]) was used. Cupric sulfate ($CuSO_4$, Sigma, purity ≈ 99%) was used as precursor to obtain Cu-based nanoclusters. Phenol (C_6H_5OH, Fulka), 2-propanol ($CH_3CH(OH)CH_3$, Sigma-Aldrich, 99.5%), methanol (CH_3OH, ACS reagent, ≥ 99.8%), acetic acid (CH_3COOH, Wako, 99.7%), and deionized water (Milli-Q with 18.6 MΩ) were used.

2.2. Photocatalyst Preparation: Modification of TiO_2-P25 by Radiolysis

The photocatalysts were synthesized by radiolytic reduction of Cu^{2+} ions. TiO_2-P25 was put in suspension in an aqueous solutions containing Cu^{2+} ($1x10^{-3}$ M) (the loading of copper was 0.5 wt%, 1 w% and 2 w%) and 2-propanol (0.1 M) (used to scavenge oxidizing $HO^{\bullet}$ radicals generated by water radiolysis)[32]. The suspensions were deaerated with nitrogen gas under stirring for 20 minutes, and then irradiated for 3.5 hours with a ^{60}Co panoramic gamma source with a dose rate of 2.3 kGy h^{-1} (dose = 8 kGy). When aqueous solutions are irradiated by high energy radiation such us γ-rays, X-rays or electron beams excitation and ionization of water takes place as following:[33]

$$H_2O \xrightarrow{\gamma-ray} e_s^-, H_3O^+, H^{\cdot}, HO^{\cdot}, H_2, H_2O_2 \qquad (1)$$

Indeed, high energy radiation of water leads to the formation of solvated electrons (e^-_s) (which are strong reducing species (E^0 (H_2O/ e^-_s = -2.87V_{NHE})) and free radicals: $H^{\bullet}$ (E^0 ($H^+/H^{\bullet}$)= -2,3 V_{NHE} and $HO^{\bullet}$ (E^0 ($HO^{\bullet}/H_2O$)= +2,8 V_{NHE}).[32] Strong oxidative hydroxyl radicals $HO^{\bullet}$ [E^0 ($^{\bullet}OH$ /H_2O) = + 2.34 V_{NHE} at pH 7] are also generated.[34] Alcohols (such as 2-propanol) are added to the solutions to scavenge oxidation hydroxyl radicals leading to formation of alcohol reducing radicals. [26,33]

$$CH_3CHOHCH_3 + HO^{\bullet} \rightarrow CH_3C^{\bullet}OHCH_3 + H_2O \quad k_1 = 1.9x10^9\ Lmol^{-1}s^{-1} \qquad (2)$$

$$CH_3CHOHCH_3 + H^{\bullet} \rightarrow CH_3C^{\bullet}OHCH_3 + H_2 \quad k_2 = 7.4x10^7\ Lmol^{-1}s^{-1} \qquad (3)$$

The alcohol radicals formed by reactions (2) and (3) are reducing agents: E^0 (($(CH_3)_2CO$/$(CH_3)_2C^{\bullet}OH$) = –1.8 V_{NHE} at pH 7. Therefore, these secondary radicals are able to directly reduce metal ions with mono- and multi-valence into a zero valence. Cu^{2+} are reduced on TiO_2 by e^-_s and $(CH_3)_2C^{\bullet}OH$ radicals induced by solvent radiolysis.[29,35] Solvent radiolysis generates a homogeneous distribution of solvated electrons and reducing radicals leading to homogeneous reduction and nucleation. Therefore, metal nanoparticles of homogeneous size are obtained.[26,32] The radiolytic reduction mechanisms of copper ions have been already described in other publications.[35] The dose used for irradiation is the dose necessary to reduce Cu^{II} into Cu^0 on TiO_2. At this dose, TiO_2 is not affected by irradiation and there is no reduction of Ti^{IV+}. The formed Cu^0 clusters on TiO_2 will be oxidized in contact with air. It is known that copper nanoclusters are sensitive to oxygen and are very fast oxidized in air leading to formation of small CuO clusters. [26,35,36,37]

The Cu-modified TiO_2-P25 photocatalysts were separated by centrifugation and dried at 60 °C for 18 h. The supernatant was completely transparent after centrifugation, indicating that all the Cu-based nanoclusters were deposited on TiO_2-P25.[26,32] The

modified materials present a light green color. The samples were labeled as P25, CuO_x/P25, where x is the mass loading in copper.

2.3. Materials Characterization

The heterojunctions CuO@TiO_2 were characterized by high angle annular dark field scanning transmission electron microscopy (HAADF-STEM). For the observations, the samples were dispersed in 2-propanol by sonication, and then dropped on a gold coated holey carbon grids. We used a Cs corrected JEOL-ARM-200F electron transmission microscope at 200 kV. Line-scan profiles Energy-dispersive X-ray spectroscopy (EDS) measurements were obtained with an Oxford detector.

For X-ray Photoelectron Spectroscopy (XPS) analysis, the samples were deposited on carbon films fully covered in order to avoid powder release. At the pressure lower than 10^{-7} torr on the analysis chamber. High resolution scans were taken for five elements, and number of scans differed depending on each element content in the sample, i.e., 50 scans were taken for Ti and O, 100 scans for C and 300-500 scans for Cu. using a JEOL JPS-9010MC with Mg Kα radiation and a hemispherical electron energy analyzer.

For Diffuse Reflectance Spectroscopy (DRS), a UV-Vis-NIR spectrophotometer equipped with an integrating sphere from Agilent Technologies Cary 5000 model was used with KBr as reference sample.

For Time Resolved Microwave Conductivity (TRMC) measurements, a pulsed and tunable (220–2000 nm) laser source with an optical parametric oscillator (OPO) EKSPLA, NT342B and a microwave generated by a Gunn diode (30 GHz) were used. This technique used to study the dynamics of photogenerated charge-carriers under UV and visible irradiation was described in previous papers.[5,6,15]

2.4 Photocatalysis Activity Test

2.4.1. Phenol Degradation under Visible Light

Phenol was used as model pollutant in water (C_6H_5OH, 50 ppm). Its photodecomposition was studied in a 10-mm light path quartz cell reactor containing 3.5 mL of the phenol solution and 1 g L^{-1} of photocatalyst. The photocatalyst was dispersed in the solution by sonication and kept under stirring for 10 min under dark conditions to reach the equilibrium between adsorption and desorption. Then, the solutions were

irradiated with a xenon lamp (Oriel 300W) and a cut-off filter (AM-32603-1, LOT-Oriel) ($\lambda > 450$ nm) was used. The photocatalytic tests were conducted under oxygen bubbling at a fixed rate flow.

Sampled aliquots of 0.5 mL were taken from the irradiated suspensions at different time intervals. The catalyst powders were separated from the solutions by centrifugation. The solutions were analyzed by High Performance Liquid Chromatography (HPLC, Agilent 1260 infinity quaternary LC) equipped with a UV-detector set at 260 nm for phenol analysis. An isocratic mobile phase consisted of 80% H_2O and 20% acetonitrile (ACN) for elution at 1 mL min^{-1} flow rate.

2.4.2. 2-Propanol Degradation under Visible Irradiation

The photodecomposition of 2-propanol was carried out in a reactor, where 15 mL of the liquid suspensions containing 50 mg of photocatalyst was dispersed in 5 mL of 2-propanol (5 v%), and covered with a septum to avoid the evaporation of acetone. The photocatalyst was irradiated for 3 h using a xenon lamp and a cut-off filter (Y48, Asahi Techno Glass) with wavelengths above 450 nm ($\lambda \geq 450$ nm) and under magnetic stirring (1000 rpm). To control the reaction temperature at 25 °C, the reactor was immersed into a water bath. Every hour the sample was taken from the reactor, filtrated using (Whatman Mini-UniPrep, PVDF) and analyzed by gas chromatograph equipped with a flame ionization detector (GC-FID; Shimadzu GC-14B). The reaction was followed by the amount of acetone generation according to the reaction:[38]

$$2(CH_3)_2CHOH + O_2 \rightarrow 2(CH_3)_2O_2 + 2H_2O \qquad (5)$$

2.4.4. Photocatalytic Production of Hydrogen (H_2)

The photocatalytic reduction reaction was performed through methanol dehydrogenation (H_2 evolution) in a closed Pyrex glass reactor. 2 mg of each photocatalyst were suspended in 2 mL of degassed aqueous solution containing 25 v% of methanol (used as a sacrificial agent) added under argon atmosphere. The photocatalyst was dispersed in the solution by sonication for 30 s and kept under vigorous stirring. The quantity of hydrogen produced was determined by a Bruker Scion GC/MS gas chromatography (GC) with a column: Mol. Sieve 5 A 75 m x 0.53 mm I.D., flow rate 22.5 mL min^{-1}, oven temp. 70 °C, detector temperature of 200 °C under argon carrier gas). LEDs (Innotas Elektronik) with wavelengths of 400 and 470 nm were used as irradiation sources.

2.4.5. Study of stability under visible light

The stability of the photocatalysts with cycling was analyzed for the photodecomposition of phenol. The resultant supernatants (aliquots of 1 mL at different irradiation times and for different cycles for 8 h irradiation) were analyzed by HPLC. The powder after different cycles was dried at 60 °C overnight, the collected samples were weighed and reused (1 mg/1 mL ratio), after each cycle.

3. Results and discussion

STEM observations of the modified titania show small Cu-based nanoclusters (around 1-3 nm), homogenously dispersed on the surface of the TiO_2-P25, as shown in Figure 1. Similar sizes of CuO nanoclusters were observed for the samples with 1% and 2% loadings. The HAADF-STEM images for Cu-based nanoclusters show arrangements of crystallographic planes, corresponding to CuO. Crystallographic planes and the FFT (fast Fourier transformation) can be observed. The measure of the interplanar spacing (*d*) was found to be equal to 0.2 nm, which corresponds to the interplanar distance for (11-1) planes of CuO according to JCPDS file no. 48-1548.[39]

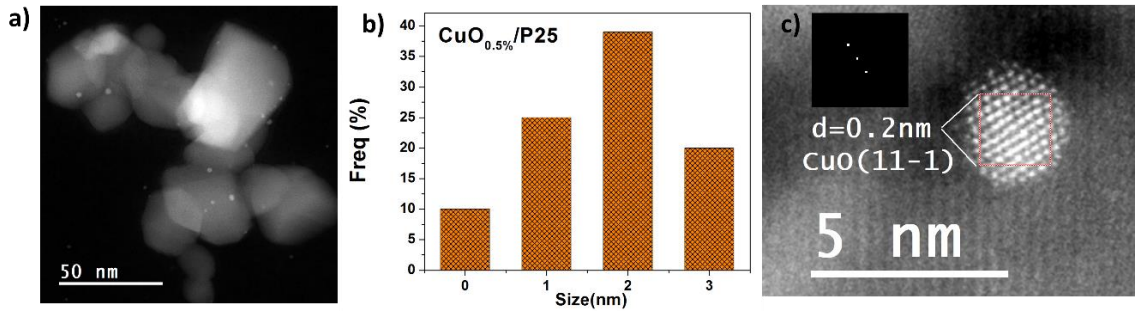

Figure 1. TEM images of ***a)*** *$CuO_{0.5\%}$/P25 with* ***b)*** *the corresponding histogram of the size distribution of CuO nanoclusters, and* ***c)*** *HAADF-STEM of BF-STEM images of, $CuO_{0.5\%}$/P25 with FFT (fast Fourier transform) images for the planes of CuO.*

The composition of the CuO-nanoclusters was determined by STEM-Electron Dispersive X-ray Spectroscopy (EDS). Different clusters were analyzed: The line profile spectra across the different individual nanoclusters show the presence of Cu (L and K) as well as Au (L and M) from the grids (Figure S1).

The analysis of the chemical composition of the modified TiO_2-P25 was carried out by XPS: The core level signals of: Cu, Ti, O and C were observed. The results are presented in Figure

S2 and Table S1. The characterization by XPS demonstrates the presence of the Ti*2p* peaks characteristic of Ti^{4+} in TiO_2 at 459.8 and 465.6 eV related to Ti$2p_{3/2}$ and Ti$2p_{1/2}$ orbitals, other peaks at 531.2 eV are attributed to O*1s* of TiO_2, and an additional peak at 284.8 eV is attributed to C1s peaks (signal obtained from the carbon films). In Cu core peaks, two components Cu$2p_{1/2}$ and Cu$2p_{3/2}$ are observed.[40] Concerning Cu$2p_{3/2}$ core levels, the E_B positions are in the range of 933.4 eV. The copper position range agrees with Cu^{2+} chemical state. but the characteristic shake-up of Cu^{II} ions is naught or very weak. The shake-up decreases with the reduction of Cu^{II} (into Cu^{I} and Cu^{0}), but is also sensitive to the particle size of Cu^{II}-based NPs.[41] Previous studies have reported that the energy position of the rising Cu K-edge of the XANES spectra of these nanoclusters corresponds to Cu^{II} species.[15]

The DRS spectra of the modified samples exhibit a slight shift in the absorption toward visible light, compared with the TiO_2-P25 that present and absorption around 400 nm[42] as shown in Figure 2. This shift is related to the equilibrium of the conduction band of TiO_2-P25 by the junction with the CuO-nanoclusters. These nanoclusters are responsible of the large absorption band in the IR with a maximum at 800 nm related to $2E_g \rightarrow 2T_{2g}$ inter-band transitions in the Cu^{II}-based clusters on TiO_2.[43] These absorption results in light green color of the samples.

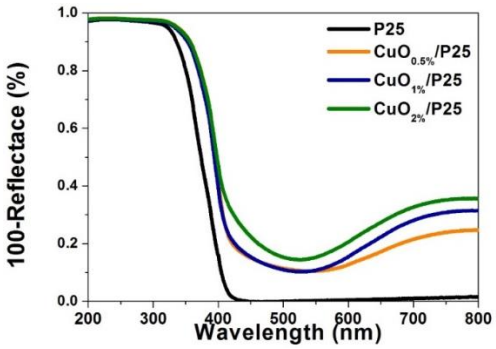

Figure 2. UV-Vis Diffused reflectance spectra of TiO_2-P25 and modified TiO_2-P25 with different loadings in CuO-nanoclusters.

The TRMC signals are shown in Figure 3. The samples were excited at fixed wavelengths under visible regions 450, 480, and 550 nm. TiO_2-P25 modified with CuO-nanoclusters exhibit strong TRMC signals under visible light. These samples exhibit higher I_{max} values compared to bare TiO_2-P25 excited with wavelengths within the visible range (450 nm, 480 nm, and 550 nm). At 450 nm, all the CuO containing samples show signals at similar I_{max} values. However, the samples show different signal decays: The decay is slower with decreasing the amount of CuO, indicating that the recombination of photogenerated charge-carriers is slower. At 480 nm, the

samples still present signals with similar I_{max} values and signals' decay. However, at 550 nm, the I_{max} value of the signals increases with the CuO loading. The signal decrease with Cu0.5% is slower indicating more charge carriers in this sample.

These TRMC results shed light on the photocatalytic mechanisms involved in TiO_2-P25 modified with CuO- nanoclusters under visible light irradiation, due to its narrow band-gap (1.7 eV).[18] TRMC signals are higher with Cu-TiO_2 samples excited under visible light indicating higher charge carriers and more electrons in the CB of TiO_2. The CuO-nanoclusters attached at the surface are able to activate the TiO_2 photocatalyst through a heterojunction between p-type CuO and n-type TiO_2 (Figure 3d). Depending on the band positions of those two semiconductors and the formed heterojunction, the photoexcited electrons are transferred from CB(CuO) to CB(TiO_2) until the Fermi levels of the semiconductors reach the same value: Electron transfer between the semiconductors due to the favorable energetics of the relative positions of the CBs, reducing significantly the electron-hole recombination probability and increasing electron lifetimes. In this case, hot electrons transferred to TiO_2 can then reduce electron acceptors to drive photocatalytic reactions. The positive holes remaining in CuO have almost no oxidation ability, because the VB level in CuO is located more cathodic than the VB of TiO_2, and therefore it is impossible to expect that those positive holes can be active. It has to be noted that the energy band-gap value decreases with the size of CuO clusters: Ge *et al*. reported that their band-gap decreases from 2.6 eV to 1.4 eV when their size increases from 1.1 nm to 2 nm.[44]

Another possible mechanism reported by Irie et al. is through interfacial charge transfer (IFCT) (Figure 3e), electrons in the VB of TiO_2 can be excited and injected to the CB of CuO.[45, 46] In this case the CB in TiO_2 is only slightly higher than oxygen-reduction potential and excited electrons in CuO may not reduce electron acceptors in one-electron reduction mode. In this case, two-electron reduction of oxygen may happen to induce visible-light photocatalysis and active holes created in the VB of TiO_2 oxidize the electron donors. This mechanism is less likely, because it would lead to trapped charge carriers and lower TRMC signals with Cu-TiO_2 samples, while the contrary is observed.

CuO activate TiO_2 in a wide range of wavelengths under visible light irradiation inducing a higher photocatalytic activity in the visible region.

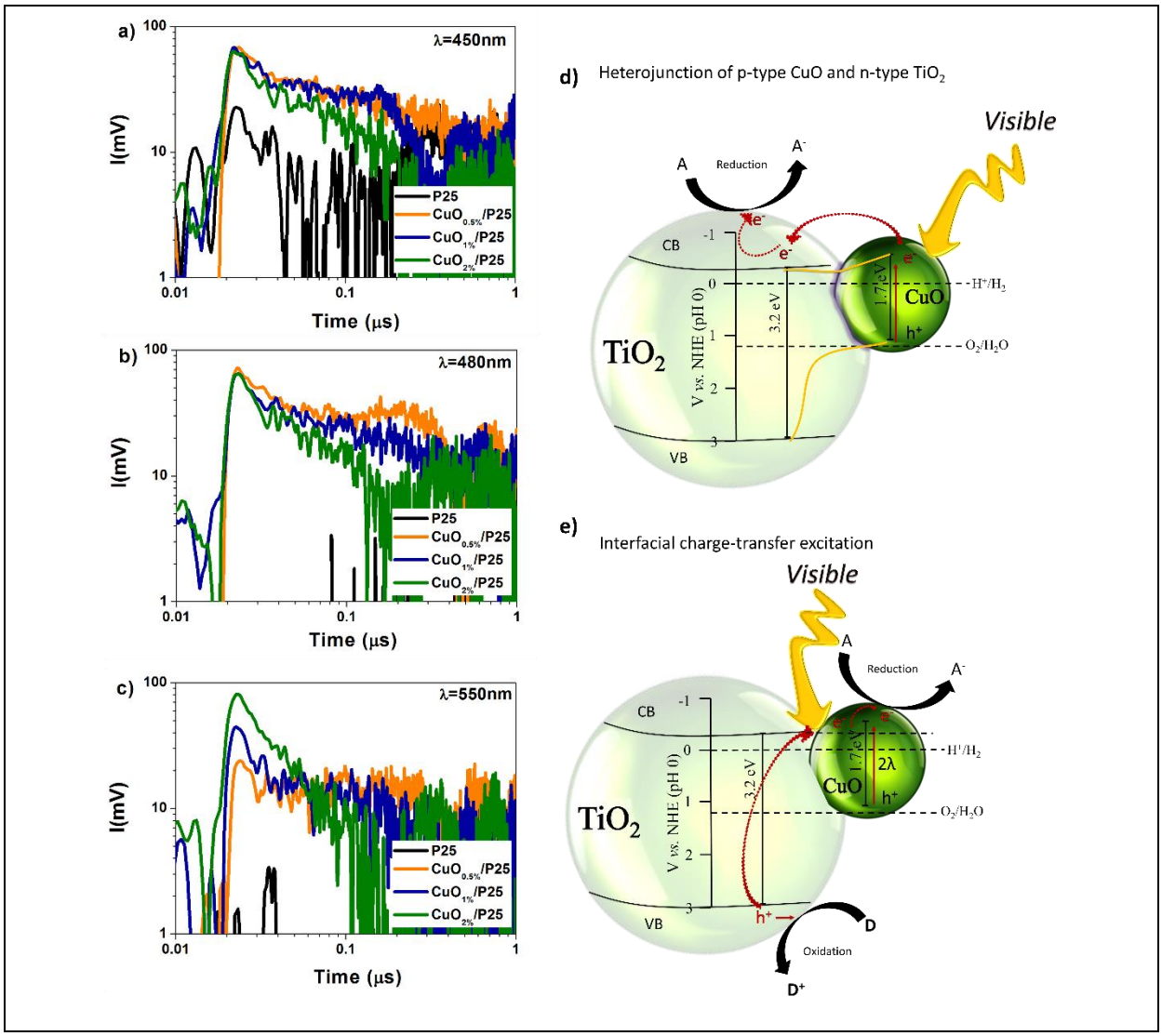

Figure 3. TRMC signals of bare and modified TiO_2-P25 with different loadings in CuO-nanoclusters after excitation at different wavelengths: ***a)*** *450,* ***b)*** *480, and* ***c)*** *550 nm, the corresponding laser energies were 6.1, 5.8, and 4.5 mJ.cm^{-2} respectively. And* ***d-e)*** *The mechanisms proposed for TiO_2-P25 modified with CuO-nanoclusters under visible light.*

4. Photocatalysic tests

4.1. Phenol and 2 propanol degradation under visible light irradiation

The photoactivity of the samples was tested for hydrogen production and degradation of model pollutants (phenol and 2-propanol) under visible light.

The photodegradation curves of phenol and 2 propanol (by acetone production) are shown in Figure 4. For phenol degradation process, it is well-known that by photocatalysis complete mineralization is obtained.[47] Phenol degradation rate with irradiation time is shown in Figure 4a. A clear enhancement on the photoactivity of TiO_2-P25 was observed under visible light

irradiation (wavelengths higher than 450 nm). The photoactivity depends on the loading with CuO clusters and the best performance is obtained with the low loading in CuO-nanoclusters for $Cu_{0.5\%}$/P25 sample. The photoactivity of bare TiO_2-P25 under visible light is usually very low because the illumination energy is lower than its band-gap energy, and its low photoactivity is related to the presence of rutile phase in TiO_2-P25.[31]

For 2-propanol degradation (Figure 4b), only acetone is detected as intermediate as is shown in equation 1. The modification with the lower amount of CuO (0.5%) leads here again to a slightly higher photocatalytic activity compared to the modification with 1% and 2% of CuO-nanoclusters. Surface modification with copper oxide nanoclusters induces a modification of the absorption properties of the TiO_2-P25 and particularly an enhancement of the absorption in the visible range creating an activity under visible light.

It is clear that, for photooxidation of organic compounds, higher photoactivity is obtained with the smaller amount of CuO nanoclusters. And this photocatalytic response can be correlated with the TRMC signals of the photocatalysts previously discussed: The $CuO_{0.5\%}$/P25 samples showed the highest I_{max} value (compared to that obtained with bare TiO_2-P25) at 450 nm, which represents more electrons in the conduction band of the semiconductor TiO_2. And for the $CuO_{0.5\%}$/P25 the decrease of the signal is lower, which refers to low recombination process and more charge carriers.

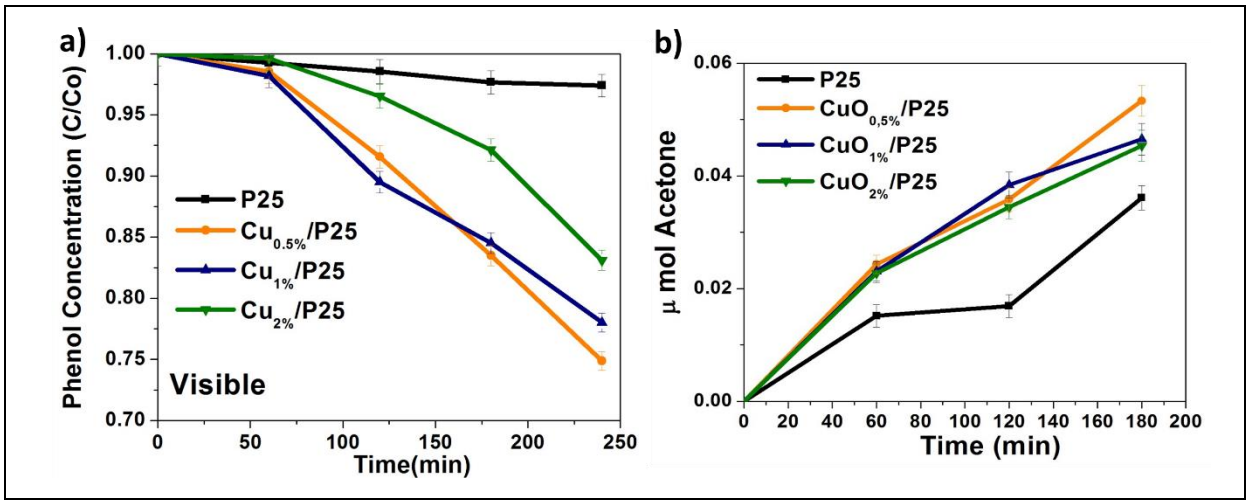

Figure 4. ***a)*** *Degradation curve of Phenol under visible light irradiation > 450 nm* ***b)*** *2-propanol degradation followed by the amount of acetone generated under visible light > 450 nm with bare TiO_2-P25 and TiO_2-P25 modified with different loading of CuO-nanoclusters.*

4.4. Photocatalytic hydrogen generation

Injected electrons in the conduction band of TiO_2 can reduce H^+ into H_2, while the holes on the surface of the semiconductor are scavenged by the methanol present in the solution. Methanol reacts with the photo-generated holes, and thus decreasing the charge carriers' recombination rate and enhancing the photocatalytic production of hydrogen by two processes (*i*) H^+ reduction and (*ii*) methanol dehydrogenation.[48,49] Hydrogen production tests under visible light at λ=470 nm (results shown in Figure 5) confirm that modification of TiO_2 with small CuO-nanoclusters induces its activation under visible light. Almost no hydrogen is detected with bare TiO_2-P25 and $CuO_{0.5\%}$/P25. However, with higher loading in CuO, hydrogen generation increases. It has to be noticed that $CuO_{0.5\%}$/P25 was the best sample for photooxidation/degradation of organic compounds. This can be explained by TRMC analysis which shows different behaviors of electron injection depending of the wavelength excitation: For $CuO_{0.5\%}$/P25, more electrons are injected at lower wavelengths in the CB of TiO_2, while for $CuO_{1\%}$/P25 and $CuO_{2\%}$/P25 more injections of electrons are obtained at higher wavelengths. CuO nanoclusters can undergo possible reduction of during hydrogen production reaction to zero-valent copper. Indeed, previous studies have shown that the Cu^{2+} species are reduced to Cu^{1+} during the hydrogen generation process, and then after irradiation time, the formation of zero-valent copper occurs.[50] This previous study on copper-modified TiO_2 and $ZrTiO_4$ points out that the photocatalysts undergo dramatic modifications leading to the real working systems quite different from the starting ones.[50] H_2 evolution can be explained by a synergic effect due to the presence of the CuO (or Cu_2O)/TiO_2 heterojunction and of metallic copper clusters.

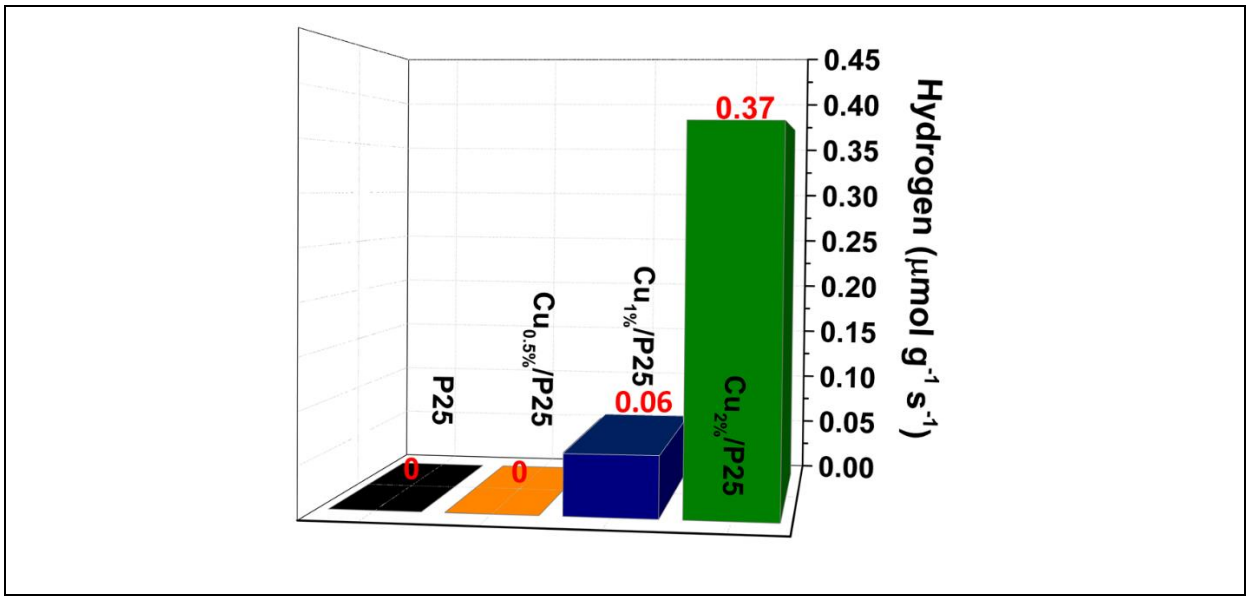

Figure 5. Photochemical H_2 generated with a LED at λ=470 nm with bare and CuO-modified TiO_2-P25 after 4h irradiation.

4.5. Stability with cycling

The stability of the photocatalysts after cycling under visible light (λ≥450 nm) was studied for phenol degradation (see Figure S3a for the sample $CuO_{0.5\%}$/P25). The photoactivity decreases after three cycles. The samples were characterized after three cycles. XPS analysis shows that the peaks corresponding to the binding energy of $Cu2_p$ core levels decreases (before disappearing) with cycling (Figure 31b). STEM images (Figure S3 c,d,e) show that (3 cycles) after the second cycle some aggregations of Cu-based nanoclusters were observed, whereas after the third cycle TiO_2 was free of CuO nanoparticles, and thus leaching of Cu was proved (Figure S3e). It is known that Cu nanoclusters are not stable at nanoscale. The loss of the $Cu2_p$ XPS signal and a decrease in the photocatalytic activity is due to Cu leaching. Moreover, copper oxides are susceptible to photocorrossion (in contrast to stable titania),[51] and thus the stability of CuO/TiO_2-based systems should be improved before possible commercialization.

Conclusions

In conclusion, small CuO nanoclusters (1-3nm) were synthesized by radiolysis on the surface of TiO_2-P25. This modification leads to an enhancement in the photocatalytic activity of TiO_2-P25 under visible light. Modification of TiO_2 with CuO nanoclusters leads to a good photocatalytic activity under visible light. For photooxidation and degradation of organic pollutants, the best results are obtained with the lowest loading in CuO, while for hydrogen

generation the activity increases with the CuO content. TRMC characterization of modified titania shows strong signals under visible light excitation due to electron transfer from CuO nanoclusters into the conduction band of TiO_2. This electrons' injection efficiency depends on the excitation wavelength and on the loading. However, in aqueous media the samples are not very stable. In further studies, stabilization of these nanoparticles against oxidation must be considered, e.g., by preparation of CuO(core)/TiO_2(shell) nanostructures. These composite nanomaterials might find other applications, e.g., in gas phase for air treatment, self-cleaning surfaces or CO_2 reduction.[16] Indeed, CuO has highly negative CB capable of reduce CO_2 to methanol or formaldehyde.[52] However, if it is irradiated under visible light electrons from CB of CuO are going to CB of TiO_2. The possibility to reduce CO_2 is reduced. Semiconductors with narrower bandgap should be used to obtain reduction of CO_2 under visible light or in the case of titania, irradiation UV should be applied.

† **Supplementary Material**: HRTEM image and EDS analysis performed on CuO nanoparticles, additional XPS analysis and binding energies of the composite CuO_x/TiO_2, photocatalytic phenol degradation with cycling and characterization of the recycled photocatalysts by XPS and STEM analysis.

ACKNOWLEDGEMENTS

Financial support from the CNRS, ECOS-Nord M11-P02 project (CNRS-CONACYT bilateral project), the CONCERT-Japan Joint Call on Efficient Energy Storage (European Commission 31671PB), the COST Nanoalloys and CONACYT (Mexico grant numbers 106437, 216315 and 356872) are highly acknowledged. Also, thanks to the National Laboratory for Nanoscience and Nanotechnology (LINAN-IPICYT) for granted infrastructure for the materials characterization, and to the Dr. Mariela Bravo for XPS measurements. M.G.M.M. acknowledges Campus France for the Eiffel Excellence Scholarship. The authors acknowledge also C'Nano Ile de France, the RTRA Triangle de la Physique, and the ANR project UpPhotoCat for the financial support for TRMC setup.

DATA AVAILABLITY STATEMENTS

The data that supports the findings of this study are available within the article [and its supplementary material].

References

1 K. Hashimoto, H. Irie, and A. Fujishima, Jpn. J. Appl. Phys. **44**, 8269 (2005).
2 K. Nakata and A. Fujishima, J. Photochem. Photobiol. C Photochem. Rev. **13**, 169 (2012).
3 B. Ohtani, Phys Chem Chem Phys **16**, 1788 (2014).
4 N.-L. Wu and M.-S. Lee, Int. J. Hydrog. Energy **29**, 1601 (2004).
5 M.G. Méndez-Medrano, E. Kowalska, A. Lehoux, A. Herissan, B. Ohtani, S. Rau, C. Colbeau-Justin, J.L. Rodríguez-López, and H. Remita, J. Phys. Chem. C **120**, 25010 (2016).
6 C. Colbeau-Justin, M. Kunst, and D. Huguenin, J. Mater. Sci. **38**, 2429 (2003).
7 X. Chen and S.S. Mao, Chem. Rev. **107**, 2891 (2007).
8 J. Yu, Y. Hai, and M. Jaroniec, J. Colloid Interface Sci. **357**, 223 (2011).
9 D. Liu, Y. Fernández, O. Ola, S. Mackintosh, M. Maroto-Valer, C.M.A. Parlett, A.F. Lee, and J.C.S. Wu, Catal. Commun. **25**, 78 (2012).
10 Z. Hai, N.E. Kolli, D.B. Uribe, P. Beaunier, M. José-Yacaman, J. Vigneron, A. Etcheberry, S. Sorgues, C. Colbeau-Justin, J. Chen, and H. Remita, J. Mater. Chem. A **1**, 10829 (2013).
11 S. Linic, P. Christopher, and D.B. Ingram, Nat. Mater. **10**, 911 (2011).
12 D. Sánchez-Rodríguez, M.G. Méndez Medrano, H. Remita, and V. Escobar-Barrios, J. Environ. Chem. Eng. **6**, 1601 (2018).
13 N. Helaïli, Y. Bessekhouad, A. Bouguelia, and M. Trari, J. Hazard. Mater. **168**, 484 (2009).
14 S. Xu and D.D. Sun, Int. J. Hydrog. Energy **34**, 6096 (2009).
15 M.G. Méndez-Medrano, E. Kowalska, A. Lehoux, A. Herissan, B. Ohtani, D. Bahena, V. Briois, C. Colbeau-Justin, J.L. Rodríguez-López, and H. Remita, J. Phys. Chem. C **120**, 5143 (2016).
16 M.G. Méndez-Medrano, E. Kowalska, M. Endo-Kimura, K. Wang, B. Ohtani, D. Bahena Uribe, J.L. Rodríguez-López, and H. Remita, ACS Appl. Bio Mater. **2**, 5626 (2019).
17 Z. Hai, N.E. Kolli, J. Chen, and H. Remita, New J. Chem. **38**, 5279 (2014).
18 R. Marschall, Adv. Funct. Mater. **24**, 2421 (2014).
19 E. Kowalska, M. Janczarek, L. Rosa, S. Juodkazis, and B. Ohtani, Catal. Today **230**, 131 (2014).
20 M. Janczarek, Z. Wei, M. Endo, B. Ohtani, and E. Kowalska, J. Photonics Energy **7**, 012008 (2016).
21 M. Jung, J. Scott, Y.H. Ng, Y. Jiang, and R. Amal, Int. J. Hydrog. Energy **39**, 12499 (2014).
22 Y. Lan, Y. Xie, J. Chen, Z. Hu, and D. Cui, Chem. Commun. **55**, 8068 (2019).
23 Slamet, H.W. Nasution, E. Purnama, S. Kosela, and J. Gunlazuardi, Catal. Commun. **6**, 313 (2005).
24 M. Janczarek and E. Kowalska, Catalysts **7**, 317 (2017).
25 M. Janczarek, K. Wang, and E. Kowalska, Catalysts **8**, 240 (2018).

26 J. Belloni, M. Mostafavi, H. Remita, J.-L. Marignier, and and M.-O. Delcourt, New J. Chem. **22**, 1239 (1998).
27 R.P. Doherty, J.-M. Krafft, C. Méthivier, S. Casale, H. Remita, C. Louis, and C. Thomas, J. Catal. **287**, 102 (2012).
28 E. Kowalska, H. Remita, C. Colbeau-Justin, J. Hupka, and J. Belloni, J. Phys. Chem. C **112**, 1124 (2008).
29 E. Grabowska, A. Zaleska, S. Sorgues, M. Kunst, A. Etcheberry, C. Colbeau-Justin, and H. Remita, J. Phys. Chem. C **117**, 1955 (2013).
30 J.F. Wishart and B. Rao, *Recent Trends in Radiation Chemistry* (WORLD SCIENTIFIC, 2010).
31 B. Ohtani, O.O. Prieto-Mahaney, D. Li, and R. Abe, J. Photochem. Photobiol. Chem. **216**, 179 (2010).
32 H. Remita and S. Remita, in *Recent Trends Radiat. Chem.* (World Scientific, 2010), pp. 347–383.
33 J. Belloni, Catal. Today **113**, 141 (2006).
34 Ferradini, C. and Pucheault, J., in *Biol. L'action Rayonnem. Ionis. Masson Paris* (Masson, Paris, 1983).
35 J. Khatouri, M. Mostafavi, J. Amblard, and J. Belloni, Chem. Phys. Lett. **191**, 351 (1992).
36 A.A. Zezin, V.I. Feldman, S.S. Abramchuk, G.V. Danelyan, V.V. Dyo, F.A. Plamper, A.H.E. Müller, and D.V. Pergushov, Phys. Chem. Chem. Phys. **17**, 11490 (2015).
37 S. Chettibi, N. Keghouche, Y. Benguedouar, M.M. Bettahar, and J. Belloni, Catal. Lett. **143**, 1166 (2013).
38 E. Kowalska, O.O.P. Mahaney, R. Abe, and B. Ohtani, Phys. Chem. Chem. Phys. **12**, 2344 (2010).
39 S.-D. Seo, Y.-H. Jin, S.-H. Lee, H.-W. Shim, and D.-W. Kim, Nanoscale Res. Lett. **6**, 397 (2011).
40 J.P. Espinós, J. Morales, A. Barranco, A. Caballero, J.P. Holgado, and A.R. González-Elipe, J. Phys. Chem. B **106**, 6921 (2002).
41 C.C. Chusuei, M.A. Brookshier, and D.W. Goodman, Langmuir **15**, 2806 (1999).
42 G.L. Chiarello, E. Selli, and L. Forni, Appl. Catal. B Environ. **84**, 332 (2008).
43 G. Colón, M. Maicu, M.C. Hidalgo, and J.A. Navío, Appl. Catal. B Environ. **67**, 41 (2006).
44 Y. Ge, Z.H. Shah, C. Wang, J. Wang, W. Mao, S. Zhang, and R. Lu, ACS Appl. Mater. Interfaces **7**, 26437 (2015).
45 H. Irie, K. Kamiya, T. Shibanuma, S. Miura, D.A. Tryk, T. Yokoyama, and K. Hashimoto, J. Phys. Chem. C **113**, 10761 (2009).
46 H. Irie, S. Miura, K. Kamiya, and K. Hashimoto, Chem. Phys. Lett. **457**, 202 (2008).
47 L.S. Andrade, E.A. Laurindo, R.V. de Oliveira, R.C. Rocha-Filho, and Q.B. Cass, J. Braz. Chem. Soc. **17**, 369 (2006).
48 J.A. Ortega Méndez, C.R. López, E. Pulido Melián, O. González Díaz, J.M. Doña Rodríguez, D. Fernández Hevia, and M. Macías, Appl. Catal. B Environ. **147**, 439 (2014).
49 M. Ni, M.K.H. Leung, D.Y.C. Leung, and K. Sumathy, Renew. Sustain. Energy Rev. **11**, 401 (2007).
50 V. Polliotto, S. Livraghi, A. Krukowska, M.V. Dozzi, A. Zaleska-Medynska, E. Selli, and E. Giamello, ACS Appl. Mater. Interfaces **10**, 27745 (2018).
51 M. Janczarek, M. Endo, D. Zhang, K. Wang, and E. Kowalska, Mater. Basel Switz. **11**, (2018).
52 S. Qin, F. Xin, Y. Liu, X. Yin, and W. Ma, J. Colloid Interface Sci. **356**, 257 (2011).